Pol. J. Environ. Stud. Vol. 32, No. 2 (2023), 1353-1370
DOI: *10.15244/pjoes/156470* ONLINE PUBLICATION DATE: 2022-12-29

Original Research

Research on Multi-Parameter Portable Water Quality Detection System Based on ZYNQ Image Processing Technology

Bingyang Sun*, Shunsheng Yang, Chen Yu

Faculty of Civil Engineering, Southwest Jiaotong University, Chengdu, 610031, China

Received: 28 September 2022
Accepted: 11 November 2022

Abstract

Combined with photoelectric detection technology and UV-Vis absorption spectroscopy in spectral analysis technology, a multi-parameter portable surface water quality detection system is developed, which can quickly detect phosphate, nitrite, and chemical oxygen demand (COD) and ammonia nitrogen water quality parameters on site. For the substances in the water body that absorb the characteristic wavelengths in the visible part, a camera is used to collect the visible spectrum, and the grayscale image of the visible spectrum image is modeled by a convolutional neural network. The concentration value of substances whose absorption characteristic wavelength is in the ultraviolet band is measured by photoelectric detection technology. The established convolutional neural network model is transplanted into ZYNQ, combined with ultraviolet photoelectric sensor, the concentration value of the detected substance is displayed on the LCD, so as to realize the economy, portability, real-time and rapidity of the water quality detector. Research indicates: The prediction value of convolutional neural network is obtained as the tendency value of sample solution in 8 output types of concentration value, the highest accuracy is 100%, and the lowest is 40%. The highest error of COD concentration value is 10%, which proves that the detection system has practical value with low noise and high precision.

Keywords: UV-Vis absorption spectroscopy, water quality testing, convolutional neural network, grayscale model

Introduction

Pollution of surface water and eutrophication of rivers and lakes are environmental issues of great concern worldwide. Robust and frequent water quality testing is the basis for safe water, food supply, production, industrial activities, etc. [1-3]. Water quality testing is fundamental to water environment management and protection, design and water treatment [4-6]. The water quality detection method in the laboratory has the advantages of high detection accuracy and complete variety of water quality parameters, but the detection process will use a variety of chemical reagents, and the detection time is too long, which is likely to cause secondary pollution. And after on-site sampling, preservation of water samples, transportation and other links, water quality

*e-mail: s20017300005@my.swjtu.edu.cn

testing is no longer real-time [7]. If the water quality is abnormal, the most suitable time for water treatment will be delayed, making it difficult to meet the needs of on-site testing of water quality in remote areas [8]. The automatic water quality monitoring station is fixed in the mainstream area, and there are few stations in small water sources and grass-roots water bodies, which do not have wide applicability [9].

The study of ultraviolet absorption spectroscopy has entered a period of rapid development. A detection system for *in-situ* real-time measurement has emerged, which simultaneously measures COD, nitrate and other parameters through UV-Vis spectroscopy [10]. An ultraviolet spectrum water quality analyzer with DSP as the processing chip, focusing on the detection of COD concentration [11]. Smartphones are combined with spectroscopic analysis technology to realize the biological detection of lysine [12]. In order to compare other color identification methods, a water quality metal ion detection method based on three primary colors and color difference formula was proposed [13]. The automatic measurement system based on spectrophotometry and flow batch analysis technology can automatically measure nitrite in seawater, etc., but it is not convenient to carry [14]. Monochromatic light is obtained through the motor-controlled spectroscopic system, and photoelectric detection is used to measure nitrate, chemical oxygen demand and total phosphorus [15]. Using the mobile phone camera as the photosensitive element, the relationship model between the water quality index concentration and the image is established, and the detection of common inorganic pollutants such as ammonia nitrogen and orthophosphate in water is realized, but the organic matter in the ultraviolet band cannot be detected [16].

At present, the mainstream methods of water quality detection technology are still photoelectric detection technology, spectral analysis technology and remote sensing detection technology [17]. Compared with traditional chemical methods, electrochemical methods, chromatography, mass spectrometry, biosensing and other water quality detection methods, water quality detection technology based on spectroscopy is more widely used in modern water quality detection systems [18]. The related research has received more and more attention and attention, and it is an important research direction of modern water quality testing technology. Among them, UV-Vis spectrophotometry is currently the mainstream water quality detection method [19]. Remote sensing techniques can be used to monitor water quality parameters turbidity, chlorophyll, and temperature [20, 21], and multiple regression analyses have assessed associations between fecal and nitrate pollution and drinking water sources [22].

Spectroscopic technology has the advantages of high accuracy, stable results, and short analysis time, and is widely used in many fields such as chemical industry, agriculture, and medicine [23]. The appearance of spectrophotometer is of great significance. As an important substance concentration detection instrument in the laboratory, it has the advantages of high sensitivity, lower stray light, high stability, stronger reliability, and more accurate analysis [24]. However, due to the need to operate in the laboratory, requiring personnel to be on duty, and not being portable, some of them are difficult to automate, and it is difficult to meet the on-site testing needs of water quality in remote areas. Portable water quality testing methods can reduce the cost of testing, shorten the testing time, and on-site water quality testing in remote areas is an urgent problem that needs to be solved now [25].

Based on various problems of traditional water quality detectors and the status quo and needs of water quality testing [26, 27]. In this paper, the Zynq system-on-a-chip of Xilinx Company is used as the basic platform, and a fast and portable water quality detection system is developed based on the principle of UV-Vis absorption spectroscopy, combined with photoelectric detection technology and spectral analysis technology. Realize on-site rapid detection of phosphate, nitrite, chemical oxygen demand, and ammonia nitrogen in natural water.

Materials and Methods

China Case Study Site and Sampling Instructions

The case was conducted in Longquan Lake and Longma Lake in Chengdu, China in July 2020, with 1 inspection site in Longquan Lake and 2 inspection sites in Longma Lake. Longquan Lake is a second-class drinking water reservoir in Chengdu, China. In April 2020, the construction of the Longma Lake water ecosystem was completed and the lake area was filled at the same time. The normal water level of the lake area has a total area of 613,300 square meters, the water depth of the reservoir area is 2-6 m, and the normal storage capacity is 890,000 m³. The lake area water ecology project mainly builds a self-purification ecosystem in the lake area and keeps the lake water body self-purifying. The water quality monitoring of the purification effect of the lake area's water ecosystem construction is tracking monitoring, with a total of three monitoring points. The monitoring indicators of this study are phosphate, ammonia nitrogen (NH_3-N), nitrite, and chemical oxygen demand (COD). After sampling, the UV-Vis spectrophotometer was used to detect and compare with the portable surface water monitoring system studied in this paper.

UV-Vis Absorption Spectroscopy

The UV-Vis absorption spectrum is due to the transition of valence electrons in the molecule [28]. Ultraviolet-visible light can be divided into deep ultraviolet region, ultraviolet region and visible light region, and the ranges of these three regions are

Table 1. Relationship between COD concentration value and voltage value.

COD Concentration value (mg/L)	0	1	2	4	6	8	12	16	20
Voltage value(mv)	681	674	656	651	630	604	575	537	511

different. The UV-Vis absorption spectrum can be used in two bands, the UV band and the visible band [29], When testing water quality, most of them are parameters such as ions and organic substances. As long as the absorption wavelength is within this range, efficient detection can be carried out for water bodies in various environments [30, 31].

Absorption Characteristics of Water Quality Indicators

Phosphate under acidic conditions, adding ammonium molybdate and ascorbic acid as color-developing agents, the solution will appear cyan blue, according to the principle of color complementarity, the solution absorbs orange light. In the national standard, 710 nm is often used as the characteristic wavelength of phosphate [32]. Nitrite reacts with p-aminobenzenesulfonic acid and naphthalene ethylenediamine hydrochloride in a weak acid medium, and the solution can appear purple-red. From the complementary colors, it can be seen that the solution absorbs yellow-green, and 538 nm is commonly used as the characteristic wavelength of nitrite.After the ammonia nitrogen solution reacts with sodium tartrate and Nessler reagent, an orange-yellow complex can be formed. According to the principle of color complementarity, the absorption color of the solution is blue-violet, and 420 nm is commonly used as the characteristic wavelength of ammonia nitrogen solution. Chemical oxygen demand (COD) detects the content of reducing substances that need to be oxidized in water, and most of the reducing substances in water are organic substances, which have better absorption in the ultraviolet spectral region [33], Usually 254 nm is used as the characteristic wavelength of COD.

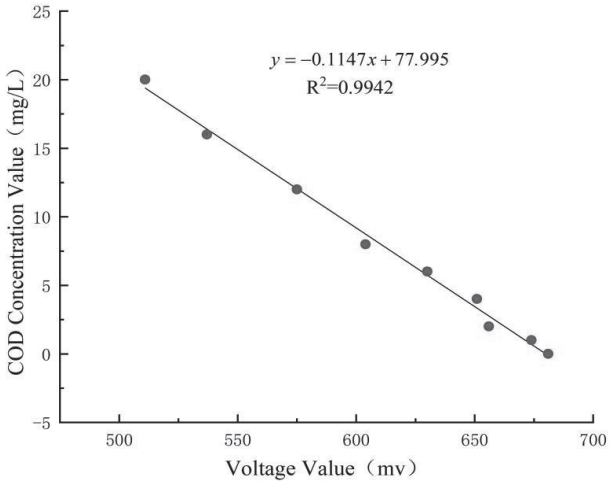

Fig. 1. Voltage value-COD concentration value fitting curve.

Commonly Used Color Quantization Models and Filtering Methods

The color quantization model is a mathematical model that uses a set of numerical values to describe the color [34]. The correct selection of the model is beneficial to image processing [35], which includes RGB quantization model, HSV quantization model, and grayscale quantization model. In image preprocessing, one of the most basic and important processing methods is image filtering [36]. Image filtering can well eliminate random noise, Gaussian noise, and salt and pepper noise caused by measurement imaging or the environment [37].

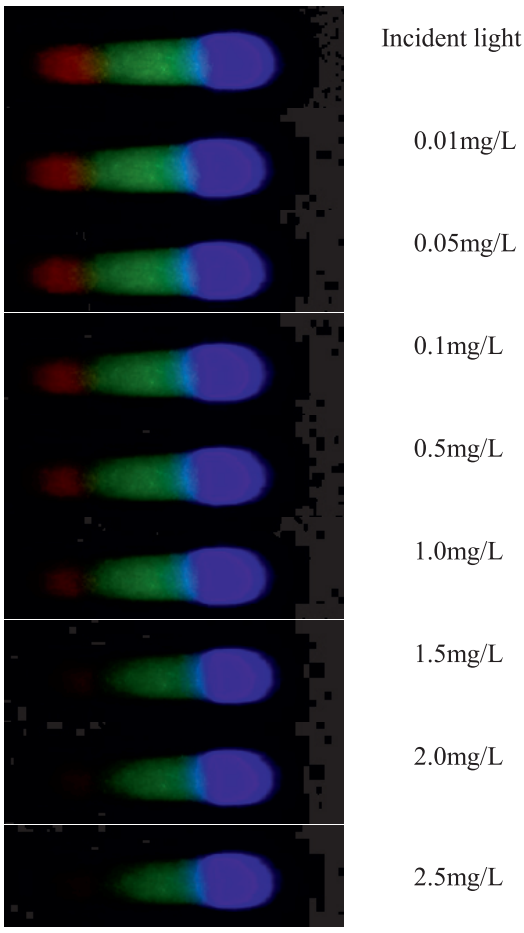

Fig. 2. Spectra of phosphate standard solutions of various concentrations.

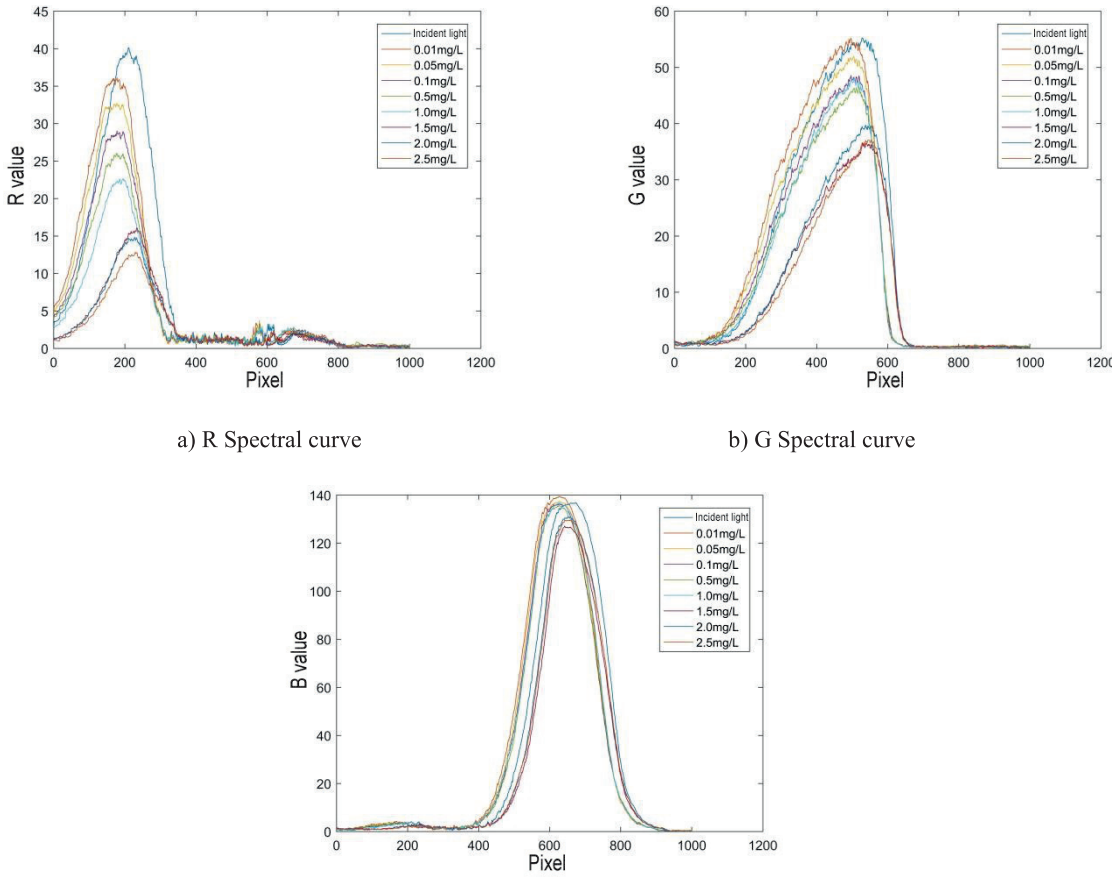

a) R Spectral curve

b) G Spectral curve

c) B SFJLk Spectral curve

Fig. 3. RGB spectrum curve of phosphate standard solution.

Simulation Modeling of Water Quality Detection System

Since the absorption characteristic wavelength of COD solution is 254 nm, it can absorb ultraviolet light [38]. The 0 mg/L blank sample and 8 different concentrations of COD standard solutions were photoelectrically detected by an ultraviolet photoelectric sensor. The 9 groups of voltage values obtained (Table 1) and the COD concentration were fitted with a single linear regression, and a single linear regression equation (Equation 2-1) could be obtained.

$$y = -0.1147x + 77.995 \tag{2-1}$$

Among them, x represents the voltage value collected by XADC, and y represents the predicted concentration value of COD. Fig. 1 is the fitting curve of voltage value and COD concentration value.

The coefficient of determination R^2 is determined by the ratio of the regression square sum to the total error square sum, which reflects the fitting degree of the regression line. The closer R^2 is to 0, the worse the fitting of the regression equation is, and the square root of the coefficient of determination is equal to the correlation coefficient. From the fitting curve of voltage value and COD concentration value, it can be seen that the correlation coefficient R is 0.9971, and the determination coefficient R^2 is 0.9942, indicating that the two have a good correlation, indicating that the model is an excellent model.

Processing and Analysis of Spectral Images

After the configuration of the standard solution is completed, add the phosphate, nitrite and ammonia nitrogen solutions to the corresponding color developer, After waiting for the color to develop, the captured image is transmitted to the PC through the camera of the detection system, and the absorption spectrum images of nitrite, phosphate and ammonia nitrogen are obtained. Image processing and curve drawing are realized by Matlab.

After processing the images of phosphate standard solutions of various concentrations through Matlab, the curves of pixels and different signal intensities can be established. The spectra of various concentrations of phosphate standard solutions are shown in Fig. 2, and the corresponding R, G, and B spectral curves are shown in Fig. 3. The phosphate standard solution after color development is blue-blue. According to the

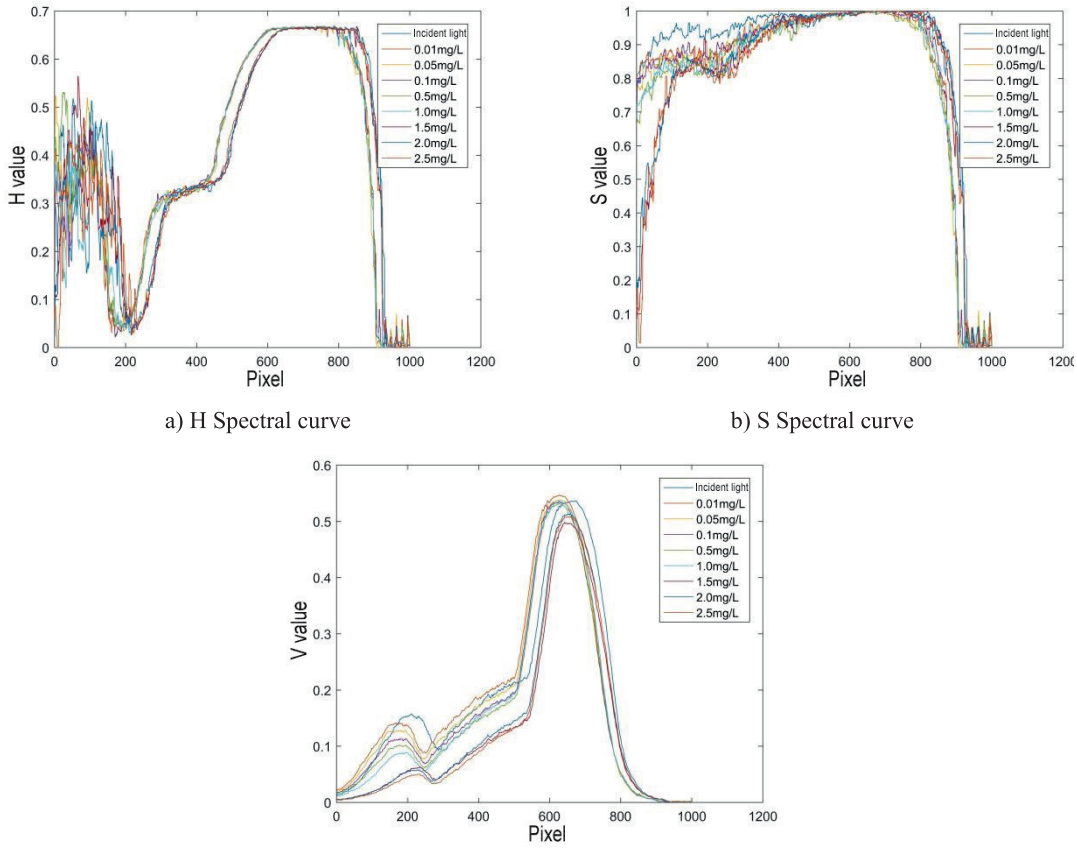

a) H Spectral curve

b) S Spectral curve

c) V Spectral curve

Fig. 4. HSV spectrum curve of phosphate solution.

theory of color complementarity, it absorbs orange light, which is similar to the 710 nm red light in the national standard. It is not difficult to find from Fig. 2 that with the increase of the concentration of the standard solution, the color of the orange to red area gradually becomes darker. It can be seen from Fig. 3 that in the orange band, the spectral curve of the R channel has a significant change, the G channel has a small change, and the spectral curve of the B channel has little change.

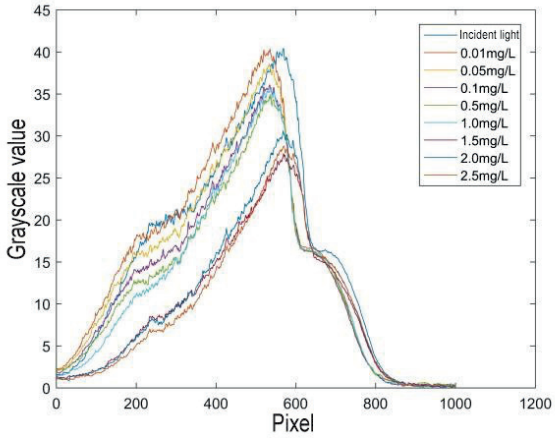

Fig. 5. Phosphate solution gray spectrum curve.

Therefore, select the quantized values at 210, 500, and 600 pixels (the pixels in this section all refer to the abscissa of the pixel point of the interception window) with large changes in the R channel, G channel, and B channel to establish the corresponding standard curve.

The H, S, and V spectral curves corresponding to each concentration of phosphate standard solution are shown in Fig. 4. Because they are all cyan and blue, there is no obvious change, so the corresponding hue H value hardly changes with the increase of concentration, as shown in Fig. 4a). The changes of the saturation S value and the lightness V value of the image with the concentration of the standard solution are shown in Fig. 4b) and Fig. 4c). It can be seen that the saturation has a large change in the red area, and there is no obvious change in other areas. In the yellow-green to red region, lightness decreases with increasing concentration, indicating that more light is absorbed in this region of the color. Therefore, 150, 100, and 200 pixels were selected for the establishment of standard curves of H, S, and V values, respectively.

The gray-scale spectral curve corresponding to each concentration of phosphate standard solution is shown in Fig. 5. It can be seen that the gray value in the green to red region also decreases as the solution concentration increases. The standard curve

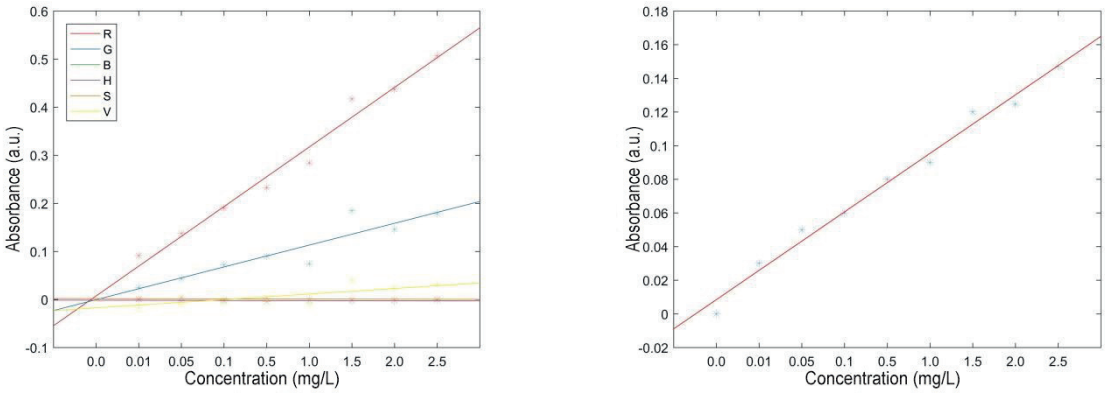

a) R, G, B, H, S,V Standard curve

b) Gray value standard curve

Fig. 6. Standard Curve of Phosphate Solution.

establishment of gray value is chosen at 500 pixels with large variation.

Therefore, the R, G, B, H, S, V and gray values at the selected pixels can be analyzed with reference to the mathematical model established by the Lambert-Beer law, and the absorbance values corresponding to different phosphate concentrations can be obtained.

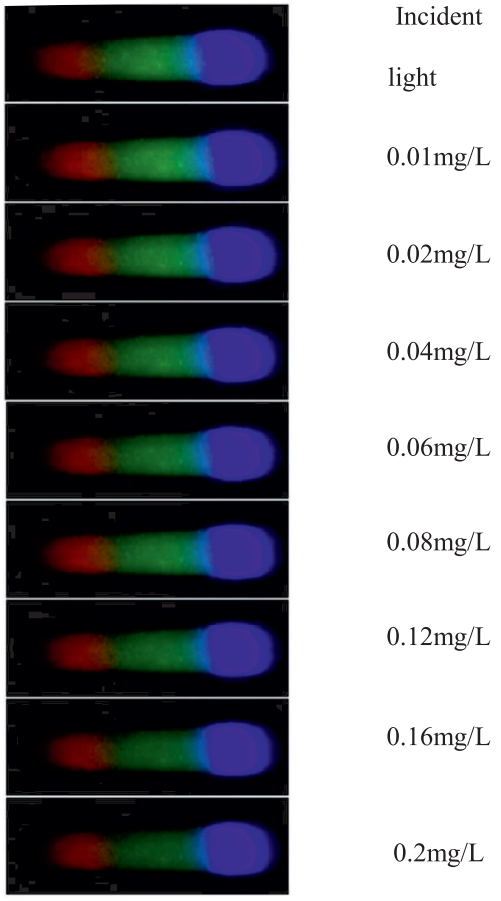

Fig. 7. Spectra of nitrite standard solutions of various concentrations.

After fitting, the standard curve shown in Fig. 6 was obtained. It can be seen from the figure that the standard curve established using the R value has the highest sensitivity, while the standard curve obtained using the H and S values has the lowest sensitivity. The slope, intercept and correlation coefficient of each standard curve are shown in Table 2, Among them, the correlation coefficients of the standard curve of R value, G value and gray value are all greater than 0.9, among which the gray value has the best correlation with the concentration of phosphate, and the other values have poor correlation. It can be seen that the model established with gray value is the best.

Similarly, the spectra of various concentrations of nitrite standard solutions are shown in Fig. 7, and the corresponding R, G, and B spectral curves are shown in Fig. 8. The nitrite standard solution after color development is purple-red. According to the theory of color complementarity, it absorbs yellow-green light, which has the same wavelength as the 538 nm yellow-green light in the national standard. It can be seen from Fig. 7 that with the increase of the standard solution concentration, the color of the yellow-green area gradually becomes darker. It can be seen from Fig. 8 that the spectral curves of the R channel and the G channel have significant changes in the orange band and the green band respectively, while the spectral curve of the B channel has little change. Therefore, the quantized values of channels R, G, and B at the pixel with the largest change amount respectively establish a corresponding standard curve.

The H, S, and V spectral curves corresponding to each concentration of nitrite standard solution are shown in Fig. 9. Because they are all purple-red hues, there is no obvious change, so the corresponding hue H value hardly changes with the increase of concentration, such as Fig. 9a). The changes of the saturation S value and the brightness V value of the image with the concentration of the standard solution are shown in Fig. 9b) and Fig. 9c). It can be seen that the saturation

Table 2. The slope, intercept and correlation coefficient of each standard curve of phosphate.

Parameter	R	G	B	H	S	V	Grayscale value
Slope	0.0620	0.0227	0.0058	-0.0002	-0.0002	0.0058	0.0174
Intercept	-0.0547	-0.0231	-0.0233	-0.0014	0.0019	-0.0233	-0.0089
Correlation coefficient	0.9422	0.9005	0.7605	-0.2555	-0.3106	0.7605	0.9932

tends to be stable over the entire spectral range, and the lightness decreases in the yellow-green region as the concentration increases, indicating that the color absorbs more light in this region. Therefore, 100, 200 and 500 pixels were selected for the establishment of standard curves of H, S, and V values, respectively.

The corresponding grayscale spectral curves of the nitrite standard solutions of each concentration are shown in Fig. 10. It can be seen that the gray value in the yellow-green area also decreases with the increase of the solution concentration. The standard curve establishment of gray value is chosen at 600 pixels with large variation.

After selecting the value pixels, analyze the R, G, B, H, S, V and gray values at the selected pixels with reference to the mathematical model established by the Lambert-Beer law to obtain the absorbance corresponding to different nitrite concentrations. The standard curve shown in Fig. 11 was obtained after a univariate linear fit. It can be seen from the figure that the sensitivity of the standard curve established by using the G value and the gray value is better, while the sensitivity of the standard curve obtained by the other values is lower. The slope, intercept and correlation coefficient of each standard curve are shown in Table 3.Among them, the correlation coefficient of the standard curve of gray value is 0.878, which indicates that the gray value has a good correlation with the concentration of nitrite, and the other values have poor correlation.

Similarly, the spectra of various concentrations of ammonia nitrogen standard solutions are shown

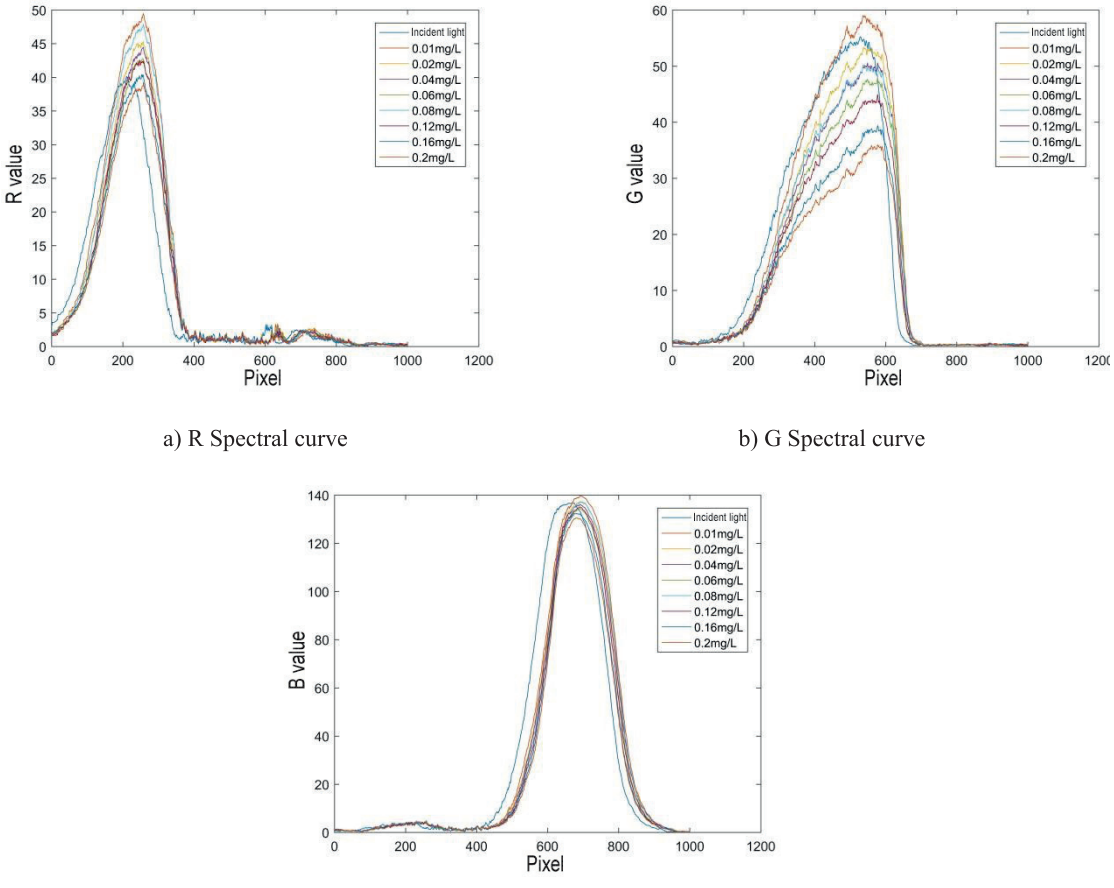

a) R Spectral curve

b) G Spectral curve

c) B Spectral curve

Fig. 8. RGB spectrum curve of nitrite standard solution.

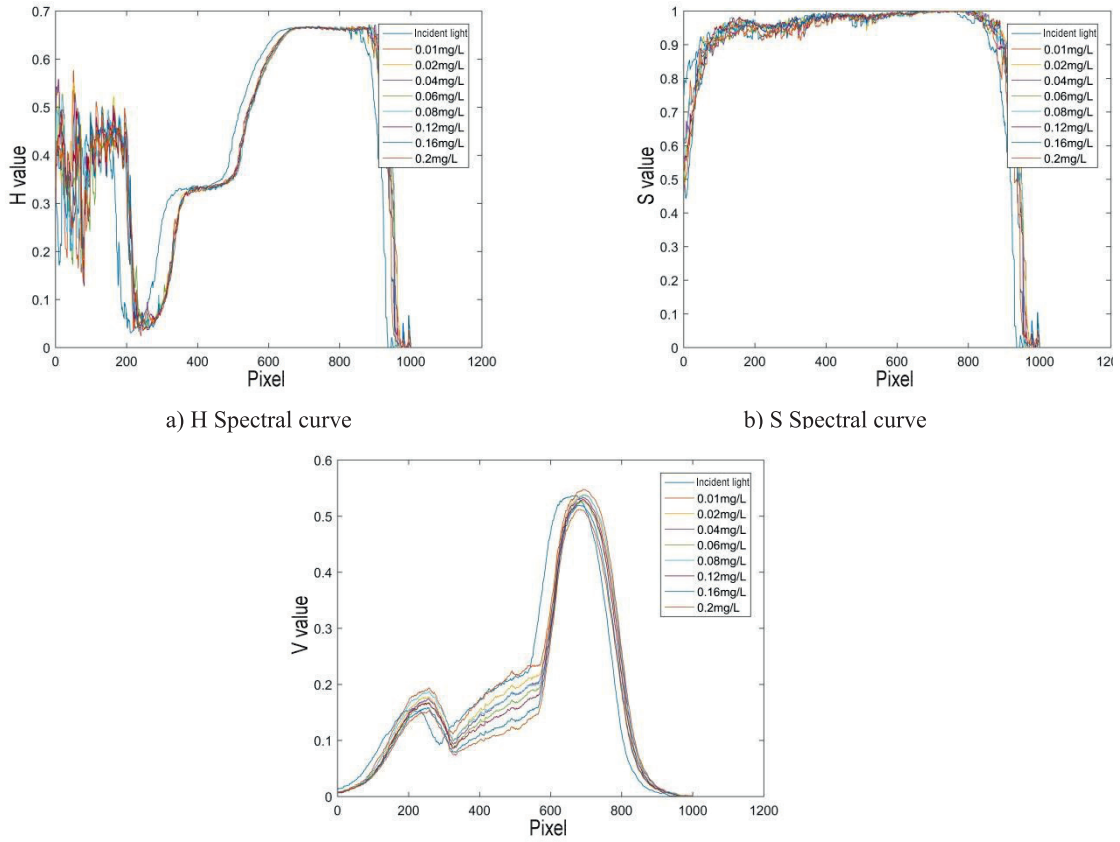

a) H Spectral curve

b) S Spectral curve

c) V Spectral curve

Fig. 9. HSV spectrum curve of nitrite solution.

in Fig. 12, and the corresponding R, G, and B spectral curves are shown in Fig. 13. The ammonia nitrogen standard solution after color development is orange-yellow. According to the theory of color complementarity, it absorbs blue-violet light, which has the same wavelength as the 420 nm blue-violet light in the national standard. It is not difficult to find from Fig. 12 that with the increase of the concentration of the standard solution, the color of the blue area gradually becomes darker. It can be seen from Fig. 13 that the spectral curves of R channel, G channel and B channel have significant changes in the orange band, yellow-green band and blue-green band, respectively. Therefore, the quantization values at 200, 550, and 700 pixels are respectively selected for the R channel, G channel, and B channel to establish the corresponding standard curve.

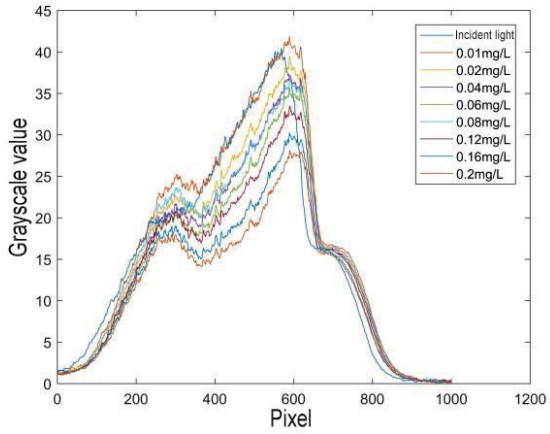

Fig. 10. Gray spectrum curve of nitrite solution.

The H, S, and V spectral curves corresponding to each concentration of ammonia nitrogen standard solution are shown in Fig. 14. Since they are all orange-yellow hues, there is no obvious change, so the corresponding hue H value hardly changes with the increase of concentration, as shown in Fig. 14a). The changes of the saturation S value and the lightness V value of the image with the concentration of the standard solution are shown in Fig. 14b) and Fig. 14c). It can be seen that in the entire spectral range, there is no significant change in saturation, and in the yellow-green and blue-green regions, the brightness decreases significantly with the increase in concentration, indicating that the color in this region absorbs more light. Therefore, 100, 100, and 700 pixels were selected for the establishment of standard curves of H, S, and V values, respectively.

Table 3. The slope, intercept and correlation coefficient of each standard curve of nitrite.

Parameter	R	G	B	H	S	V	Grayscale value
Slope	-0.0012	0.0225	0.0020	-0.0020	-0.0004	0.0020	0.0177
Intercept	-0.1167	-0.0486	-0.0163	-0.0206	-0.0067	-0.0163	-0.0688
Correlation coefficient	-0.0579	0.8272	0.5949	-0.4349	-0.3154	0.5949	0.8780

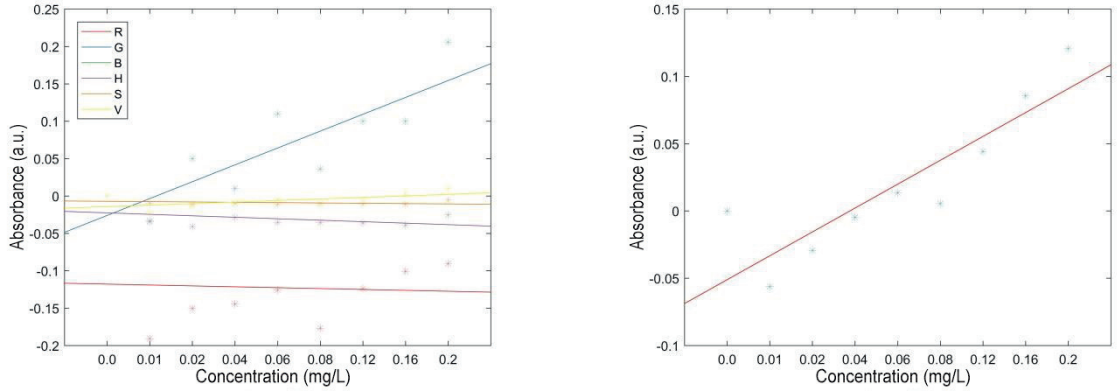

a) R, G, B, H, S, V Standard curve

b) Gray value standard curve

Fig. 11. Nitrite Standard Curve.

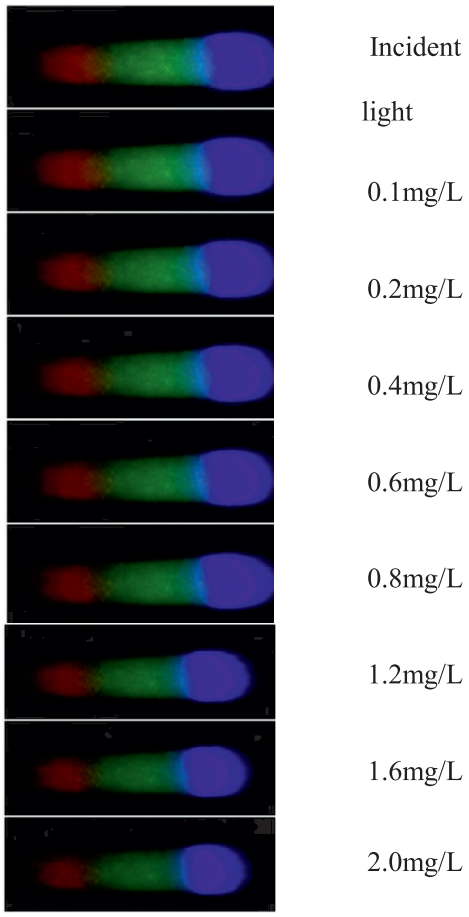

Fig. 12. Spectral diagrams of ammonia nitrogen standard solutions of various concentrations.

The gray-scale spectral curve corresponding to each concentration of ammonia nitrogen standard solution is shown in Fig. 15. It can be seen that the gray value in the green region decreases as the solution concentration increases. The standard curve establishment of gray value is chosen at 580 pixels with large variation.

After determining the value pixels, analyze the R, G, B, H, S, V and gray values at the selected pixels with reference to the mathematical model established by the Lambert-Beer law to obtain the absorbance values corresponding to different ammonia nitrogen concentrations, The standard curve shown in Fig. 16 was obtained after a univariate linear fit. It can be seen from the figure that the standard curve established using the G value has the highest sensitivity, while the standard curve obtained using the H and S values has the lowest sensitivity. The slope, intercept and correlation coefficient of each standard curve are shown in Table 4. Among them, the correlation coefficient of the gray value standard curve is greater than 0.99, indicating that the gray value has the best correlation with the concentration of ammonia nitrogen, and the correlation between H and S values are poor.

Neural Network Modeling

Convolutional Neural Networks (CNN) are mainly designed for two aspects, namely image classification and image recognition [39, 40].

The best quantification model for the absorption spectra of phosphate, nitrite and ammonia nitrogen

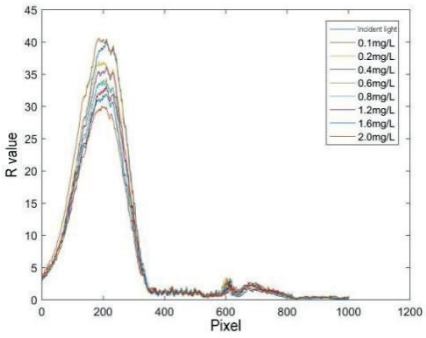

a) R Spectral curve

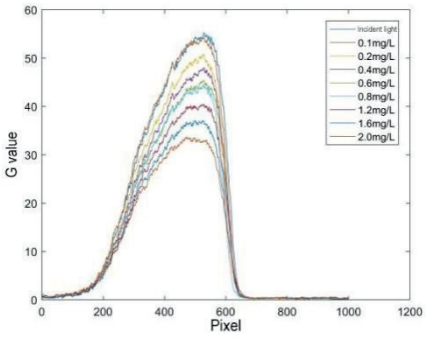

b) G Spectral curve

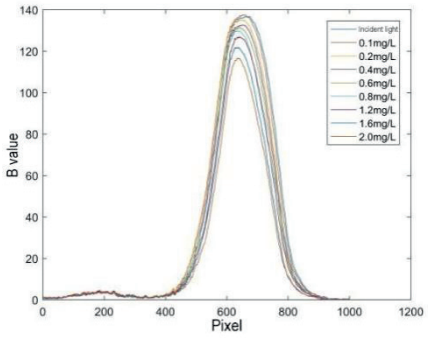

c) B Spectral curve

Fig. 13. RGB spectrum curve of ammonia nitrogen standard solution.

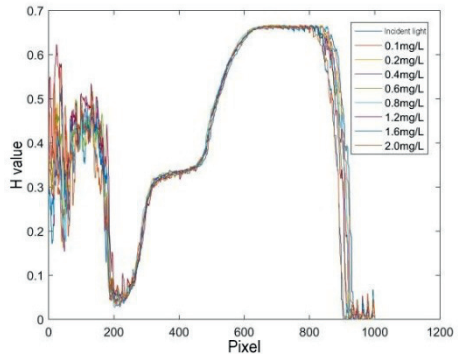

a) H Spectral curve

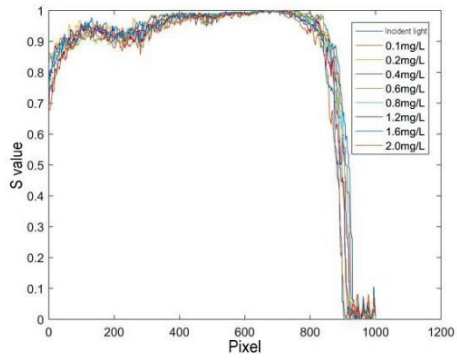

b) S Spectral curve

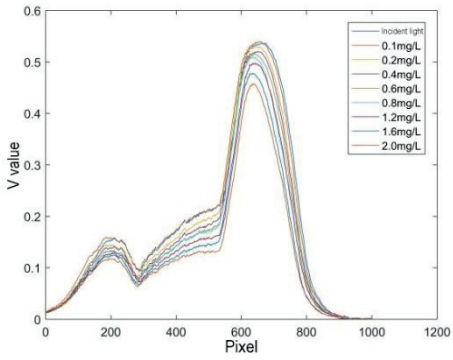

c) V Spectral curve

Fig. 14. HSV spectrum curve of ammonia nitrogen solution.

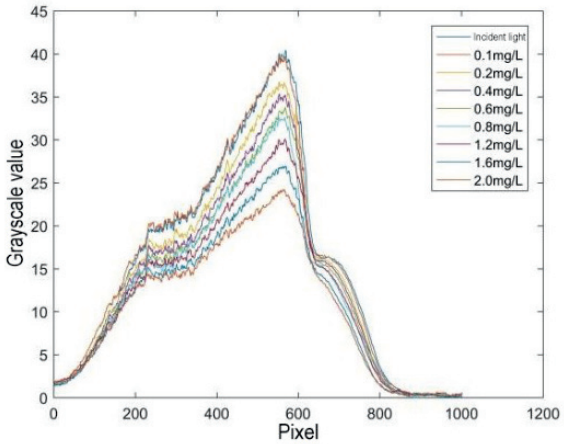

Fig. 15. Gray-scale spectrum curve of ammonia nitrogen solution.

is the grayscale model. Therefore, we can build a convolutional neural network prediction model from a grayscale image of the visible absorption spectrum [41].

The established convolutional neural network model consists of an input layer, 2 convolutional layers, 2 pooling layers, a fully connected layer and an output layer in sequence. The training set for each water quality indicator consists of 900 grayscale images, and the test set consists of 200 grayscale images. In the process of network training, by adjusting different training times, it is finally found that the best training effect is achieved when the training times are set to 100 times. The activation function uses Relu, the learning rate is set to 0.1, and each batch of training images is 20 to update the weights and biases.

The training results of Phosphate are shown in Fig. 17, the accuracy rate has reached 90%, and the error and mean square error between the maximum values of each iteration will eventually stabilize.

Similarly, the training results of nitrite can be obtained as shown in Fig. 18. The accuracy rate is 89%, and the error and mean square error between the maximum values of each iteration will eventually stabilize.

The training results of ammonia nitrogen are shown in Fig. 19, the accuracy rate is 91%, and the error and mean square error between the maximum values of each iteration will eventually stabilize.

It can be seen that the overall accuracy of the convolutional neural network prediction model has reached more than 89%, which is suitable for predicting the concentration values of phosphate, nitrite and ammonia nitrogen.

Design of Multi-Parameter Water Quality Detection System

The content and distribution of various substances in the natural water environment are constantly changing with the changes of time, location, meteorological conditions and pollution source discharge. Since the traditional water quality testing methods require on-site sampling, storage and transportation to be carried

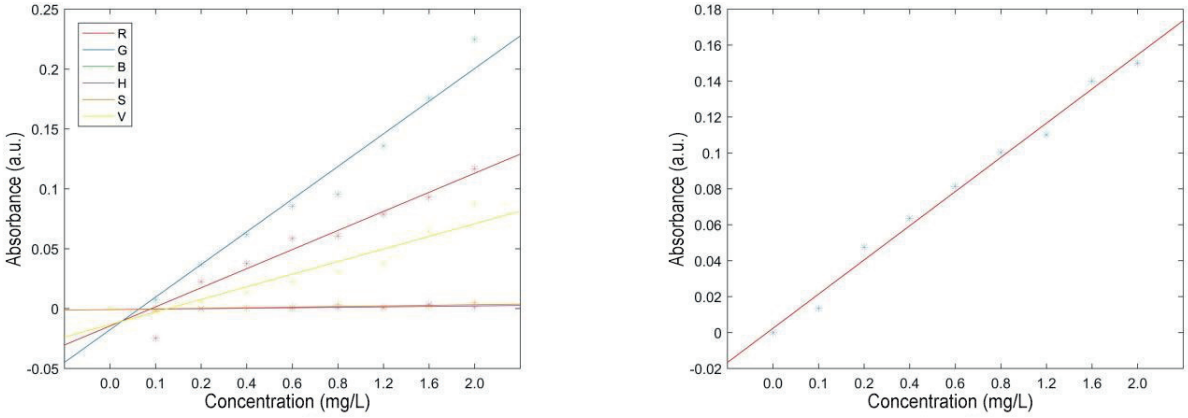

a) R, G, B, H, S, V Standard curve

b) Gray value standard curve

Fig. 16. Ammonia Nitrogen Standard Curve.

Table 4. The slope, intercept and correlation coefficient of each standard curve of ammonia nitrogen.

Parameter	R	G	B	H	S	V	Grayscale value
Slope	0.0159	0.0273	0.0105	0.0004	0.0005	0.0105	0.0190
Intercept	-0.0305	-0.0450	-0.0239	-0.0013	-0.0013	-0.0239	-0.0167
Correlation coefficient	0.9362	0.9425	0.9475	0.7454	0.7573	0.9475	0.9946

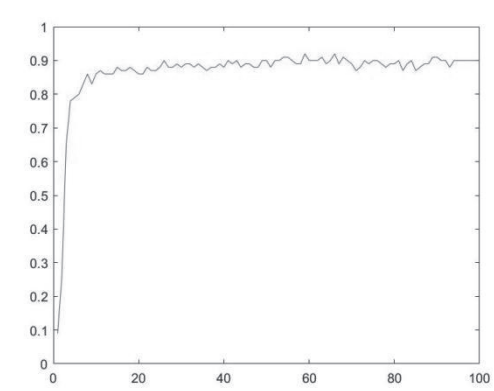

a) Accuracy

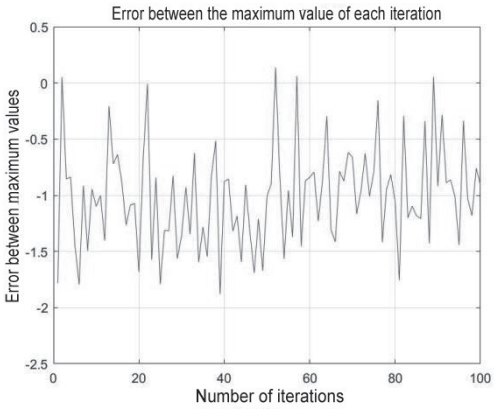

b) Error between the maximum value of each iteration

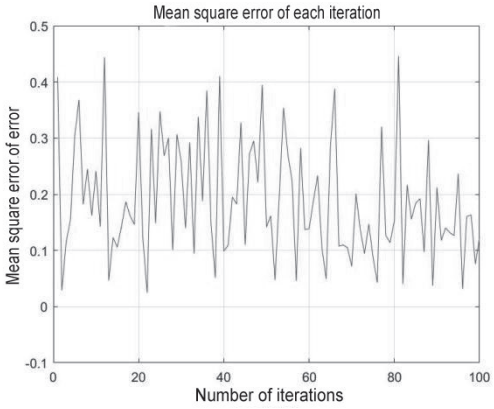

c) Mean square error of each iteration

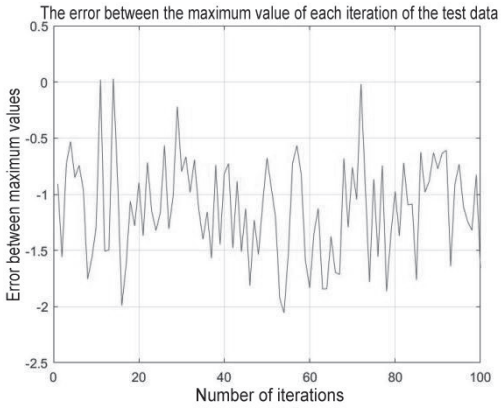

d) The error between the maximum value of each iteration of the test data

Fig. 17. Phosphate training results.

out in the laboratory, it is increasingly unable to meet the needs of water quality testing.In order to meet the needs of on-site water quality testing. The main design of the water quality detection system in this paper includes three parts: the optical path structure design, the hardware system design and the software system design, as shown in Fig. 20.

Combined with photoelectric detection technology and spectral analysis technology, the overall structure of the detection system is designed. The structure includes ultraviolet-visible light source, spectroscopic system, cuvette, camera, ultraviolet photoelectric sensor, AD conversion module, main control chip and LCD display, the sensor model is OV5640 CMOS type digital image sensor. The optical path part mainly refers to the structure of the UV-Vis spectrophotometer, Designed and implemented based on Lambert-Beer law, it consists of light source, diaphragm, plano-convex lens, cuvettes and gratings. Among them, phosphate, nitrite and ammonia nitrogen have the effect of absorbing visible light, COD has a strong absorption effect on 254 nm ultraviolet rays. So the light source uses a combined light source. The software part includes camera configuration, image data capture, Gaussian filtering, grayscale image conversion, convolutional neural network prediction, AD data acquisition, COD concentration conversion, LCD driver and LCD display interface, mainly using Vivado 19.1 as the development platform and Verilog as the programming language. The ultraviolet photoelectric sensor can convert the optical signal into an electrical signal, and after analog-to-digital conversion, it is received by the main control chip FPGA. The camera collects the visible absorption spectrum and sends it to the FPGA for processing. The software is developed through the Vivado platform, the convolutional neural network model is transplanted through the HLS platform, and the concentration value display of the detection system is completed through the LCD.

Considering the selection of UV LED and white LED dual light sources as the light source of the detection system. Among them, the white LED chooses the DC3~5V driver-free lamp bead module of Ruibao Light Technology,Powered by three AA batteries. The ultraviolet LED uses the UVC3535 deep ultraviolet lamp bead module with the characteristic wavelength of

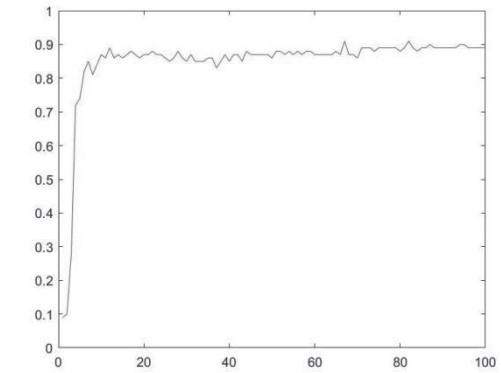

a) Accuracy

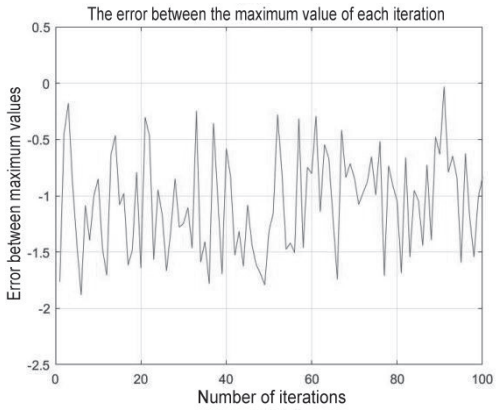

b) Error between the maximum value of each iteration

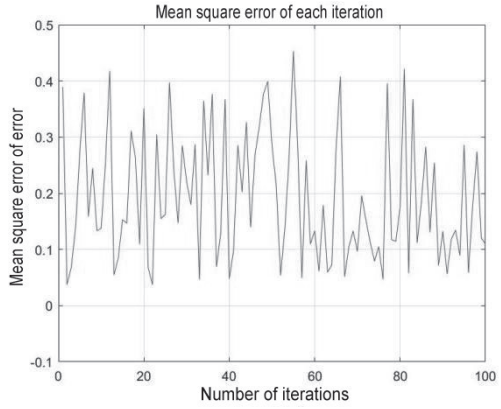

c) Mean square error of each iteration

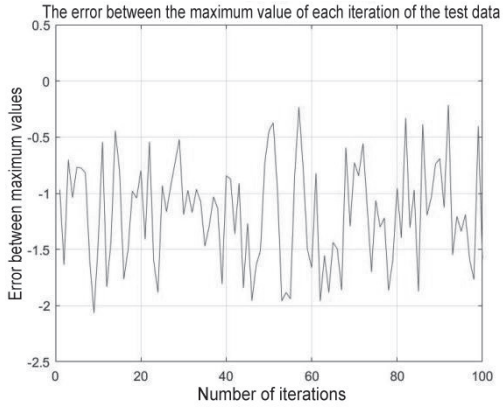

d) The error between the maximum value of each iteration of the test data

Fig. 18. Nitrite training results.

254 nm from Ruibao Lighting Technology. The input voltage is 8V, and it is powered by 2 18650 lithium batteries.

The names, models and specifications of the components of the spectroscopic system used in this system are shown in Tables 4-2.

This detection system needs to transmit ultraviolet light, so choose a quartz cuvette that can transmit ultraviolet light on both sides. The high-transmittance quartz cuvette with 10 mm optical path (Puxi Optical) is used, which can transmit light with a wavelength of 200 nm to 2500 nm, and the light transmittance is greater than 83%. It is suitable for experimental analysis of ultraviolet-visible absorption spectrum.

Considering the requirements and cost of this detection system, the CMOS type digital image sensor, model OV5640, was finally selected. The chip of the OV5640 sensor is only 0.25 inches, the photosensitive array is up to 5 million pixels, and its resolution can even reach 15fps QSXVGA (2592*1944) or 90 fps VGA (640*480) [42]. Its sensor is derived from OmniBSI technology, which greatly improves the performance of high sensitivity and low noise.

The spectral detection range is the primary consideration when choosing a photodetector. The detection system needs to detect the ultraviolet light with the wavelength of 254 nm when detecting the COD parameters, so it is necessary to select the detection device with absorption characteristics in the 254 nm band. This detection system uses an ultraviolet photoelectric sensor produced by Huanggang Yunshang Electronic Technology Co., Ltd., the model is UV254A-1808, and the real object is shown in Figs 4-8. This sensor is a calibrated analog signal output sensor. It is powered by a standard 5V power supply with low power consumption. It has 2 analog outputs. The output voltage of OUT2 is 4.3 times that of OUT1, which is convenient for the circuit application environment. One on-board precision op amp can be omitted.

In the design of this article, considering the issues of resolution and cost, the RGB LCD screen of ATK-4384 is selected. The size of this LCD screen is 4.3 inches and the resolution is 800*480.

The physical diagram and interface schematic diagram of ATK-4384 are shown in Figs 4-11.

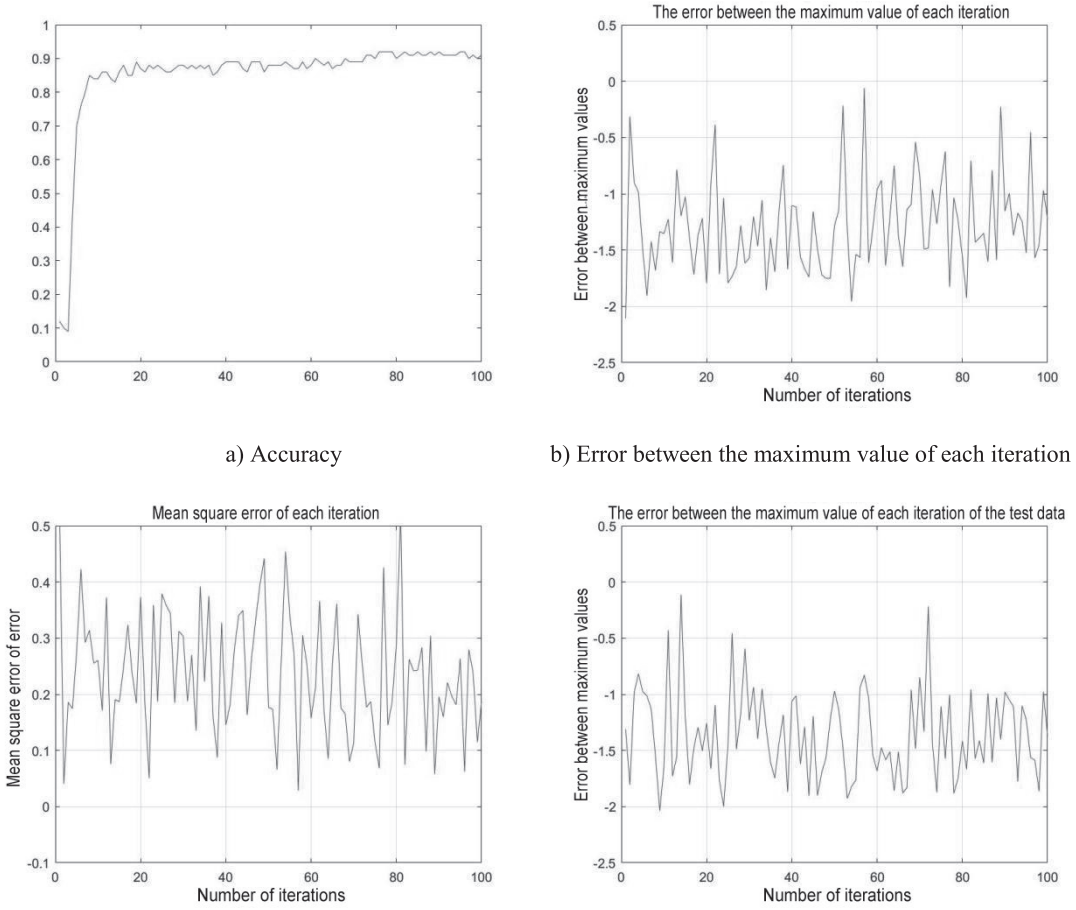

a) Accuracy

b) Error between the maximum value of each iteration

c) Mean square error of each iteration

d) The error between the maximum value of each iteration of the test data

Fig. 19. Ammonia training results.

The power supply voltage of the LCD is 5V, which can be powered by the 5V power output expansion port of the development version. R[7:0], G[7:0] and B[7:0] are 24-bit pixel data, and DE is the data enable signal, BL is the brightness adjustment signal, VSYNC is the vertical synchronization signal, HSYNC is the horizontal synchronization signal, and CLK is the pixel clock signal.

Combined with photoelectric detection technology and spectral analysis technology, the overall structure of the detection system is designed. The structure includes ultraviolet-visible light source, spectroscopic

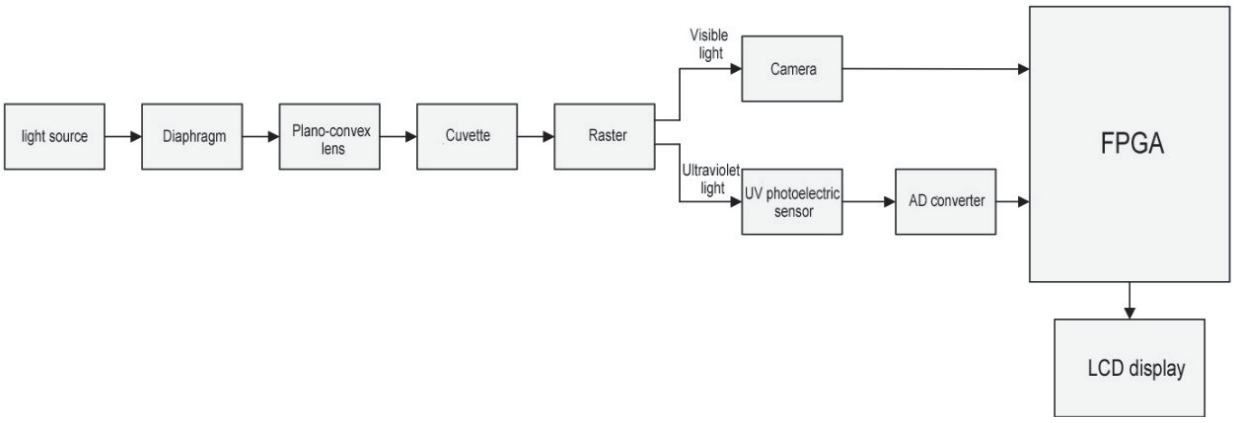

Fig. 20. Overall block diagram of the detection system.

system, cuvette, camera, ultraviolet photoelectric sensor, AD conversion module, main control chip and LCD display. The selection and use of the components of the optical path and hardware were analyzed in detail. The software was developed through the Vivado platform, the convolutional neural network model was transplanted through the HLS platform, and the concentration value display of the detection system was completed through the LCD.

Results and Discussion

On-Site Water Quality Sampling and Testing

The sample collection sites are Chengdu Longma Lake monitoring point 1, Longma Lake monitoring point 2 and Longquan Lake monitoring point 1. The collected samples were tested on-site, sampled and stored, and then sent to a water quality testing agency for testing, and the data obtained were compared.

The water quality indicators of each testing point were tested 5 times on site, and the testing institutions used spectrophotometer for testing. The testing data obtained from the three sampling points are shown in Table 5, Table 6 and Table 7 respectively.

As can be seen from the foregoing, the output types of the convolutional neural network prediction model of phosphate are 8 types, including 0.01 mg/L, 0.05 mg/L, 0.1 mg/L, 0.5 mg/L, 1.0 mg/L, 1.5 mg/L, 2.0 mg/L and 2.5 mg/L. When the phosphate content is closer to a certain classification concentration value, the predicted value is more inclined to this concentration value. For example, when the measured values of phosphate at the three monitoring points are 0.05 mg/L, 0.03 mg/L and 0.09 mg/L, the accuracy rates of predicting similar concentrations of 0.05 mg/L, 0.01 mg/L (0.05 mg/L is also a similar concentration value) and 0.1 mg/L are 100%, 60% (40%) and 80%, respectively. In the same way, the accuracy rates of the three monitoring points for predicting the approximate concentration of nitrite at 0.04 mg/L are 100%, 80%, and 80%, respectively. The accuracy rates of predicting the similar concentrations of ammonia nitrogen of 0.1 mg/L, 0.1 mg/L, and 0.2 mg/L (0.1 mg/L is also a similar concentration value) are 100%, 80% and 60% (40%). It can be seen that the closer the water quality index content is to the concentration classification value, the

Table 5. Name, model and specification of components of the spectroscopic system.

Name	Model	Specification
Diaphragm	SK12	Φ1.0-12 mm
Flat convex lens	Pu Xi Optical Quartz Plano-Convex Lenses	Φ30 mm, f39.2 mm
Holographic Diffraction grating	Yuan Qiu Technology Corporation GS012	1200 lines/mm, 20 mm*20 mm*2 mm
Lens holder	Heng Yang Optical MLNR-1.2	Φ30 mm
Grating holder	Heng Yang Optical EPH-12.5	60 mm*34.5 mm Clamping thickness 0-12.5 mm
Optical bench	Cope 25009	55 mm*42 mm*55 mm

Table 6. One-point detection results of Longma Lake monitoring.

Number of inspections	1	2	3	4	5	Spectrophotometer
Phosphate (mg/L)	0.05	0.05	0.05	0.05	0.05	0.05
Nitrite (mg/L)	0.04	0.04	0.04	0.04	0.04	0.04
Ammonia (mg/L)	0.1	0.1	0.1	0.1	0.1	0.094
COD (mg/L)	11	11	11	10	11	10

Table 7. Two-point detection results of Longma Lake monitoring.

Number of inspections	1	2	3	4	5	Spectrophotometer
Phosphate (mg/L)	0.05	0.01	0.01	0.05	0.01	0.03
Nitrite (mg/L)	0.04	0.02	0.04	0.04	0.04	0.04
Ammonia (mg/L)	0.1	0.1	0.2	0.1	0.1	0.130
COD (mg/L)	12	12	11	11	12	11

Table 8. Longquan Lake test results.

Number of inspections	1	2	3	4	5	Spectrophotometer
Phosphate (mg/L)	0.1	0.1	0.1	0.05	0.1	0.09
Nitrite (mg/L)	0.04	0.04	0.04	0.01	0.04	0.03
Ammonia (mg/L)	0.1	0.2	0.2	0.1	0.2	0.151
COD (mg/L)	13	14	13	14	13	13

more stable the prediction effect of the convolutional neural network is. The predicted value of COD concentration value is generally high, with a maximum error of 10%.

In this detection system, the absolute errors of phosphate, nitrite and ammonia nitrogen are small when the concentration value is low, and the relative error is large (up to 67%). As the concentration value increases, the relative error decreases (up to 12.5%), but the absolute error keeps increasing. The main reason for the error is the output type of the convolutional neural network, the more the output is classified, the smaller the error will be generated.

The reason why the predicted value of COD is generally higher than the actual value is because of the influence of natural water turbidity. Because in addition to the organic matter in the water that absorbs the ultraviolet light at 254 nm, the turbidity also has a certain absorption effect. In surface water with generally better water quality, turbidity has little effect on COD detection. When the water turbidity is high, the COD measurement value will be high.

Conclusions

Configure standard solutions of four water quality indicators. For the characteristic wavelengths of the absorption spectra of phosphate, nitrite and ammonia nitrogen in the visible light part, the absorption spectra of 8 standard solutions with different concentrations were collected. The standard curves under different color quantization models are established by using the Lambert-Beer law through Matlab, and the optimal conclusion of the grayscale model is obtained. The lowest correlation coefficient is 0.87, and the highest is 0.99. The convolutional neural network model was established in Matlab for the visible spectrum grayscale image, and the prediction accuracy reached 89%. Since the characteristic wavelength of COD's absorption spectrum is the ultraviolet band of 254 nm, a prediction model of voltage and concentration value was established for it by univariate linear fitting, and the correlation coefficient reached 0.99.

The field test of the detection system was conducted and compared with the laboratory test value, the convolutional neural network predicted value was the trend value among 8 concentration values, and the accuracy rate was 100% at the highest and 40% at the lowest. The maximum error of COD concentration value is 10%, and the reason for the error is analyzed.

Combining the photoelectric detection technology and the ultraviolet-visible absorption spectroscopy in the spectral analysis technology, a portable surface water quality detection system has been developed, and the detection of four water quality parameters of phosphate, nitrite, COD and ammonia nitrogen in the water quality has been completed. It has the advantages of low detection cost, short detection period, and real-time on-site detection, and has wide applicability to water quality detection in natural water bodies, especially in remote areas.

The water quality detection system is still insufficient, and can be further studied.

(1) The detection system does not realize the function of human-computer interaction. If the cost factor is not considered, the detection system can also develop in the direction of higher integration.

(2) Only four water quality indicators have been studied in this detection system, and the detection of water quality parameters can be increased to make the detection system function more perfect.

Acknowledgments

The authors thank Southwest Jiaotong University in China for their financial and technical support, and the research results of the project have been recognized by the team members of the college.

Conflicts of Interet

The authors declare no conflicts of interest.

References

1. MAZARI-HIRIART M., PONCE-DE-LEÓN S., LÓPEZ-VIDAL Y., ISLAS-MACÍAS, P., AMIEVA-FERNÁNDEZ R.I., QUIÑONES-FALCONI F. Microbiological implications of periurban agriculture and water reuse in Mexico City. PLoS One, **3** (5), e2305, **2008**.
2. GARCÍA-ÁVILA F., JIMÉNEZ-ORDÓÑEZ, M., TORRES-SÁNCHEZ J., IGLESIAS-ABAD S., CABELLO TORRES R., ZHINDÓN-ARÉVALO C. Evaluation of the

impact of anthropogenic activities on surface water quality using a water quality index and environmental assessment. Journal of Water and Land Development, 58, **2022**.
3. WRIGHT J., GUNDRY S., CONROY R. Household drinking water in developing countries: a systematic review of microbiological contamination between source and point-of-use. Tropical medicine & international health, **9** (1), 106-117.**2004**.
4. DAMO R., ICKA P. Evaluation of Water Quality Index for Drinking Water. Polish Journal of Environmental Studies, **22** (4), **2013**.
5. EDITION F. Guidelines for drinking-water quality. WHO chronicle, **38** (4), 104, **2011**.
6. SCHWARZENBACH R.P., EGLI T., HOFSTETTER T.B., VON GUNTEN U., WEHRLI B. Global water pollution and human health. Annual review of environment and resources, **35**, 109, **2010**.
7. TAKAHARA T., MINAMOTO T., DOI H. Effects of sample processing on the detection rate of environmental DNA from the Common Carp (Cyprinus carpio). Biological Conservation, **183**, 64, **2015**.
8. PELETZ R., KISIANGANI J., BONHAM M., RONOH P., DELAIRE C., KUMPEL E., MARKS S., KHUSH R. Why do water quality monitoring programs succeed or fail? A qualitative comparative analysis of regulated testing systems in sub-Saharan Africa. International journal of hygiene and environmental health, **221** (6), 907, **2018**.
9. SYU W.J., CHANG T.K., PAN S.Y. Establishment of an Automatic Real-Time Monitoring System for Irrigation Water Quality Management. International journal of environmental research and public health, **17** (3), **2020**.
10. LANGERGRABER G., FLEISCHMANN N., HOFSTAEDTER F. A multivariate calibration procedure for UV/VIS spectrometric quantification of organic matter and nitrate in wastewater[J]. Water Science & Technology, **47** (2), 63, **2003**.
11. MU X. Technical research and realization of UV full spectrum on-line water quality measuring instrument. Chengdu: University of Electronic Science and Technology, **11**, 1, **2009**.
12. GALLEGOS D., LONG K.D., YU H., CLARK P.P., LIN Y., GEORGE S., NATH P., CUNNINGHAM B.T. Label-free biodetection using a smartphone[J]. Lab on a chip, **13** (11), **2013**.
13. DONG S. Research on remote image water quality analysis and monitoring method of point source pollution based on colorimetric method. Beijing: North China University of Technology, **08**, 36, **2016**.
14. DONG C. Design of an automatic determination system for seawater nutrients based on spectrophotometry. Guilin: Guilin University of Electronic Science and Technology, **01**, 224, **2019**.
15. CHEN H. Research on multi-parameter detection system of drinking water based on UV-Vis absorption spectrum. Changchun: Jilin University, **08**, 14, **2020**.
16. WU X. Research on smartphone-based image sensing technology for detecting common pollutants in water. Shanghai: Shanghai Normal University, **07**, 22, **2020**.
17. CHEN H., ZHAO L., YU F., DU Q. Detection of phosphorus species in water: technology and strategies. Analyst, **144** (24), 7130, **2019**.
18. IGHALO J.O., ADENIYI A.G., MARQUES G. Internet of things for water quality monitoring and assessment: a comprehensive review. Artificial intelligence for sustainable development: theory, practice and future applications, 245, **2021**.
19. FIGUEIRÓ C.S.M., DE OLIVEIRA D.B., RUSSO M.R., CAIRES A.R.L., ROJAS S.S. Fish farming water quality monitored by optical analysis: The potential application of UV–Vis absorption and fluorescence spectroscopy. Aquaculture, **490**, 91, **2018**.
20. GÜRSOY Ö., ATUN R. Investigating surface water pollution by integrated remotely sensed and field spectral measurement data: A case study. Polish Journal of Environmental Studies, **28** (4), **2019**.
21. RITCHIE J.C., ZIMBA P.V., EVERITT J.H. Remote sensing techniques to assess water quality. Photogrammetric engineering & remote sensing, **69** (6), 695, **2003**.
22. CRONIN A.A., ODAGIRI M., ARSYAD B., NURYETTY M.T., AMANNULLAH G., SANTOSO H., DARUNDIYAH K. Piloting water quality testing coupled with a national socioeconomic survey in Yogyakarta province, Indonesia, towards tracking of Sustainable Development Goal 6. International journal of hygiene and environmental health, **220** (7), 1141, **2017**.
23. CHEUNG G., MAGLI E., TANAKA Y., NG M.K. Graph spectral image processing. Proceedings of the IEEE, **106** (5), 907, **2018**.
24. MORRIS R. Spectrophotometry. Current Protocols Essential Laboratory Techniques, **11** (1), 1, **2015**.
25. AARESTRUP F.M., WOOLHOUSE M.E. Using sewage for surveillance of antimicrobial resistance. Science, 367 (6478), 630, **2020**.
26. HAN H., ZHANG K., ZHANG J. Evaluating the health of an urban river combining DPSIR framework and an improved fuzzy matter-element extension model: a case study from the Jinshui River. Polish Journal of Environmental Studies, **29** (3), 2211, **2020**.
27. HUANG P., WANG K., HOU D., ZHANG J., YU J., ZHANG G. In situ detection of water quality contamination events based on signal complexity analysis using online ultraviolet-visible spectral sensor. Applied optics, **56** (22), 6317, **2017**.
28. KHVOSTENKO O.G., KINZYABULATOV R.R., KHATYMOVA L.Z., TSEPLIN E.E. The lowest triplet of tetracyanoquinodimethane via UV–vis absorption spectroscopy with Br-containing solvents. The Journal of Physical Chemistry A, **121** (39), 7349, **2017**.
29. PHILIPPIDIS A., POULAKIS E., KONTZEDAKI R., ORFANAKIS E., SYMIANAKI A., ZOUMI A., VELEGRAKIS M. Application of ultraviolet-visible absorption spectroscopy with machine learning techniques for the classification of Cretan wines. Foods, **10** (1), 9, **2021**.
30. SCARIA J., ANUPAMA K.V., NIDHEESH P.V. Tetracyclines in the environment: An overview on the occurrence, fate, toxicity, detection, removal methods, and sludge management. Science of The Total Environment, **771**, 145291, **2021**.
31. ZULKIFLI S.N., RAHIM H.A., LAU W.J. Detection of contaminants in water supply: A review on state-of-the-art monitoring technologies and their applications. Sensors and Actuators B: Chemical, **255**, 2657, **2018**.
32. KUMAR S., CHENG J., KUBAR A. A., GUO W., SONG Y., LIU S., CHEN S., TIAN J. Orange light spectra filtered through transparent colored polyvinyl chloride sheet enhanced pigment content and growth of Arthrospira cells. Bioresource Technology, **319**, 124179, **2021**.
33. CHEN J., LIU S., QI X., YAN S., GUO Q. Study and design on chemical oxygen demand measurement based on ultraviolet absorption. Sensors and Actuators B: Chemical, **254**, 778, **2018**.

34. BRUN L., TRÉMEAU A. Color quantization. In Digital color imaging handbook (pp. 589-637). CRC press, **2017**.
35. YANG X., REN T., TAN L. 2020. Size Distribution Measurement of Coal Fragments Using Digital Imaging Processing. Measurement, **2020** (160), 107867, **2017**.
36. GUO X., LI Y., SUO T., LIU H., ZHANG C. Dynamic deformation image de-blurring and image processing for digital imaging correlation measurement. Optics and Lasers in Engineering, **98**, 23, **2017**.
37. JOSHI A., BOYAT A.K., JOSHI B.K. Impact of wavelet transform and median filtering on removal of salt and pepper noise in digital images. In 2014 International Conference on Issues and Challenges in Intelligent Computing Techniques (ICICT) (pp. 838-843). IEEE, February, **2014**.
38. CHEN H., XUE H., LIU J., LI Z., HOU Y. Research on COD detection method based on UV-Vis spectroscopy. In Ninth International Symposium on Precision Mechanical Measurements (Vol. **11343**, p. 113430U). International Society for Optics and Photonics, November, **2019**.
39. CARAFA R., FANGGIANO L., REAL M., MUNNÉ A., GINEBREDA A., GUASCH H., FLO M., CARSTEN VON DER OHE P. Water toxicity assessment in Catalan rivers (NE Spain) using Species Sensitivity Distribution and Artificial Neural Networks. Science of the Total Environmental, **409**, 4269, **2011**.
40. SARIGÜL M., OZYILDIRIM B.M., AVCI M. Differential convolutional neural network. Neural Networks, **2019** (116), 279, **2019**.
41. CHEUNG G., MAGLI E., TANAKA Y., NG M.K. Graph spectral image processing. Proceedings of the IEEE, **106** (5), 907, **2018**.
42. PEI Z., PENG A. Design of image acquisition and processing system based on FPGA and OV5640. Electromechanical Information, **2019** (32), 159, **2019**.